Final-state electron-electron interaction in Compton scattering

J. A. Soininen, K. Hämäläinen, and S. Manninen
Department of Physics, POB 64, University of Helsinki, FIN-00014 Helsinki, Finland
(Received 24 April 2001; published 10 September 2001)

We introduce an analytic approximation for the spectral function, which describes the final-state electron-electron interaction in the nonresonant inelastic x-ray scattering process. We show that a relatively simple expression is adequate to characterize the excited state. We have evaluated the spectral function for various free electron densities and momentum transfer values and discuss the final state effects in the light of some recent high resolution Compton scattering experiments. It is shown that the observed smearing of the Fermi edge at relatively low incident photon energies can mostly be associated to the final state effects due to the finite width of the spectral function.

DOI: 10.1103/PhysRevB.64.125116 PACS number(s): 78.70.Ck,71.10.Ca,71.15.Qe

I. INTRODUCTION

Within the impulse approximation (IA) the cross section of inelastic x-ray scattering at the high momentum transfer limit (the so-called Compton regime) is directly related to the electronic ground state wave function via the Compton profile $J(p_z)$ defined as

$$J(p_z) = \int \int dp_x dp_y \rho(\mathbf{p}), \tag{1}$$

where $\rho(\mathbf{p})$ is the ground state electron momentum density and p_z the electron momentum component along the scattering vector $\mathbf{q}$. The IA assumes that the energy and the momentum transfers are large enough in order to treat the ejected electron as a free noninteracting particle. Most Compton scattering experiments have been interpreted within this picture using a correlated momentum density. Within this picture the Compton scattering technique offers a unique spectroscopic tool to directly access the *ground* state electronic properties of solids. Due to the advent of modern synchrotron radiation sources with powerful insertion devices, novel crystal spectrometers have been constructed to improve the momentum resolution. The resolution and the statistical accuracy have been considered to be the only limitations when the experimental results are compared with the theory. However, in many cases there have been unexplained differences implying that the experimental profiles are broader than the theoretical ones.

Several theoretical efforts to study the accuracy of the IA have been made. It is quite clear, for example, that the IA starts to break down for the tightly bound core electrons. The so-called ''Compton defect,'' which refers to the asymmetry and the shift of the Compton profile, is a good example of an IA failure. Mendelsohn and Biggs[1] and Bloch and Mendelsohn[2] calculated the shift for the *K* and *L* shell electrons by approximating the final state of the ejected electron as a continuum state in a central potential. Gasser and Tavard[3] calculated corrections to IA by making a series expansion of the Born operator. The resulting overlap integrals involved the displacement of the recoiling electrons during the collision. It turned out that this leads to a peak shift towards lower energy transfers for the *s* electrons but it can be of either sign for the *p* electrons. Bergstrom *et al.*[4] used a relativistic second-order *S*-matrix calculation within the independent particle approximation to estimate the error in the IA as a function of the incident photon energy. They concentrated on the strongly bound electrons and compared their results with experiments that used coincidence technique to isolate the desired shell contribution from the inelastically scattered spectrum. Issolah *et al.*[5] calculated the incident photon energy dependence of the Be core Compton profile using a quasiconsistent-field approach for the potential felt by the outgoing electron. A comparison with the experimental data, measured at two different incident energies, one below and one above 10 keV, gave better agreement than the impulse approximation.

The need to incorporate the electron-electron correlation into the calculation of the momentum density in the interpretation of the Compton scattering data became obvious in the analysis of the experimental results on copper by Bauer and Schneider.[6] They stressed that the band structure calculations within the local density approximation (LDA) do not yield the correct momentum density. They used a correction, which was based on the model developed by Lam and Platzman,[7] to treat the electron correlation in the inhomogeneous electron gas. Since then this correction, which is isotropic in the momentum space, has been referred to as Lam-Platzman correction. Already earlier, Lundqvist and Lyden[8] had also applied a sophisticated inhomogeneous electron gas treatment to calculate the momentum distribution and Compton profile of the interacting conducting electrons in lithium, and sodium and compared the results with the early experiments.[9] The statistical accuracy of the experiments was, however, too low to make any quantitative conclusions. Pandey and Lam[10] applied an interacting electron gas model and took into account the core-orthogonalization and the electron-ion interaction to quite successfully explain the high momentum tail in the experimental Compton profile of sodium,[11] measured using 22 keV x rays. Takada and Yasuhara[12] calculated the momentum distribution of the electron gas using an effective-potential expansion method at different free electron densities. They made an extensive comparison with the other methods in terms of the renormalization factor which is related to the size of the jump at the Fermi break. More recently, Kubo[13] calculated the momen-

tum density for lithium and sodium metals using GW approximation (GWA) (Ref. 14) obtaining a result that was in relatively good agreement with the experimental Li results of Schülke *et al.*[15] However, later GWA works by Schülke[16] and Eguiluz *et al.*[17] seem to agree with the results obtained using LDA and Lam-Platzman correction but disagreed with the experimental results. Filippi and Ceperley[18] used a pseudopotential quantum Monte Carlo simulation to calculate the directional Compton profiles for lithium. They claimed that correlation can only be responsible for about 30% of the discrepancy between the theory and the experimental data. Stutz *et al.*[19] measured the Compton profiles of disordered alloys $Li_{1-x}Mg_x$ and compared the experimental results with the theoretical ones computed using the Korringa-Kohn-Rostoker coherent-potential-approximation LDA . The agreement between the theoretical and the experimental Compton profiles improved as the Mg concentration increased. However, the heights of the peaks in the second derivative showed different qualitative behavior as a function of the concentration, the theoretical ones decreasing as the Mg concentration was increased whereas the experimental ones remained more or less independent of the alloy concentration.[19] These results seem to indicate that the observed experimental smearing of the momentum density can not be fully explained by the underestimation of the ground state correlation effects.

At the moment it is possible to have a momentum resolution of about 0.02 a.u. in the Compton scattering spectroscopy,[20] which means that detailed information on the Fermi surface, for example, can be obtained (Fermi momenta are of the order of 1 a.u.). Recent experiments with this resolution[21,22] have shown, however, that the sharp details in the Compton profiles (or in its derivatives) have been smeared significantly more than expected on the basis of the experimental resolution. Additionally, the smearing depends on the incident energy, unfortunately in such a way that the effect is larger at lower energies (around 10 keV) where the highest resolution x-ray spectrometers operate. A jellium model for including the final state interactions in Compton scattering was proposed by Schülke *et al.*[15] and it could explain most of this additional broadening in the case of lithium.[22] The observed broadening was found to be mostly due to the fact that the final state electron's spectral function has a finite width. In this work we introduce an analytical model for the spectral function, which can be used to analyze the Compton scattering results. Its importance at different incident photon energies and momentum resolutions is estimated in the case of simple metals (Li, Be, and Na). Some previously unresolved discrepancies between the theory and experiments are reconsidered in terms of the spectral function.

II. THEORY

The nonrelativistic interaction Hamiltonian between an electron system and an external electromagnetic field is

$$\mathbf{H}_{e-p}=\sum_i \left(\frac{1}{2}\alpha^2\mathbf{A}_i\cdot\mathbf{A}_i+\alpha\mathbf{p}_i\cdot\mathbf{A}_i\right), \tag{2}$$

where the summation is over the electrons in the system. $\mathbf{A}_i$ is the photon field operator and α the fine structure constant. Within the first order perturbation theory the operator $\mathbf{p}_i\cdot\mathbf{A}_i$ is responsible for the absorption and the emission processes, and the operator $\mathbf{A}_i\cdot\mathbf{A}_i$ for the scattering processes. Neglecting the absorption and emission contributions, the double differential cross section for the non-resonant inelastic x-ray scattering can be written as

$$\frac{d\sigma}{d\Omega d\omega_2}=\left(\frac{d\sigma}{d\Omega}\right)_{Th} S(\mathbf{q},\omega), \tag{3}$$

where $(d\sigma/d\Omega)_{Th}$ is the Thomson scattering cross section and $S(\mathbf{q},\omega)$ the dynamic structure factor, which depends only on the momentum $\mathbf{q}$ and the energy ω transferred to the system in the scattering process. Assuming that the IA is valid, the dynamic structure factor is related to the Compton profile in the nonrelativistic limit regime as

$$S^{\mathrm{IA}}(\mathbf{q},\omega)=J(p_z)/q, \tag{4}$$

where $p_z=(\omega-q^2/2)/q$. It was pointed out in Refs. 15 and 22 that at the high momentum transfer regime a good approximation for the dynamic structure factor would be

$$S(\mathbf{q},\omega)=\frac{2}{n}\int_{-\omega}^{0} dE \int \frac{d\mathbf{p}}{(2\pi)^3} A(\mathbf{p},E)A(\mathbf{p}+\mathbf{q},\omega+E), \tag{5}$$

where the single-particle spectral functions have been used for the final state hole, $A(\mathbf{p},E)$, and for the final state electron, $A(\mathbf{p}+\mathbf{q},\omega+E)$, and n is the average electron density of the system. The spectral functions can be written using the single particle Green's function $G(\mathbf{k},E)$ as

$$A(\mathbf{k},E)=\frac{1}{\pi}\left|\mathrm{Im}\, G(\mathbf{k},E)\right|. \tag{6}$$

Two approximations have to be made to obtain the simple expression given in Eq. (4) for the dynamic structure factor: (i) The energy E in the spectral function for the electron is replaced by $p^2/2$, i.e., the scattering is assumed to take place from a well defined quasiparticle and contributions to the scattering from plasmarons,[15] for example, are neglected. (ii) The final state electron is assumed to be a free and noninteracting particle, in which case the spectral function simplifies to a delta function $A(\mathbf{p}+\mathbf{q},\omega+E)=\delta(\omega+E-(\mathbf{p}+\mathbf{q})^2/2)$. Using these two approximations and the fact that for $\omega \gg E_f$

$$\rho(\mathbf{p})=\frac{2}{(2\pi)^3 n}\int_{-\omega}^{0} dE A(\mathbf{p},E) \tag{7}$$

the IA limit [Eq. (4)] for the dynamic structure factor is obtained. In the following we will show how the use of the spectral function for the interacting final state electron modifies this simple expression.

The dynamic structure factor within the approximation (i) becomes

$$S(\mathbf{q},\omega)=\int d\mathbf{p}\rho(\mathbf{p})A(\mathbf{p}+\mathbf{q},\omega+p^2/2). \tag{8}$$

From this expression, although it can be used once the momentum density of the system is known, it is not clear how the final state spectral function modifies the dynamic structure factor. The role of the spectral function in Eq. (8) becomes more apparent if one realizes that its shape at the high momentum regime changes quite slowly but its position follows closely the quasiparticle behavior $\omega_{\text{peak}}\propto k^2/2$. By defining a new function, which is the spectral function on a energy scale shifted by $-k^2/2$ we obtain

$$S(\mathbf{q},\omega)=\int d\mathbf{p}\rho(\mathbf{p})\tilde{A}(\mathbf{p}+\mathbf{q},\omega-\mathbf{p}\cdot\mathbf{q}-q^2/2), \tag{9}$$

where $\tilde{A}(\mathbf{k},E)=A(\mathbf{k},E+k^2/2)$. Because for large q the shape of the spectral function in Eq. (9) changes rather slowly as function of momentum, we can approximate $\mathbf{p}+\mathbf{q}\approx\mathbf{q}$ in the momentum argument to obtain

$$S(\mathbf{q},\omega)=\int d\omega' S^{IA}(\mathbf{q},\omega')\tilde{A}(\mathbf{q},\omega-\omega'). \tag{10}$$

As a result, we can see that the IA-based dynamic structure factor should be convoluted with the spectral function. This means that the final state effects determine the intrinsic resolution at which the Compton profile or the momentum density can be measured. This internal smearing depends on the momentum transfer in the scattering process and therefore also on the incident photon energy used in the experiment.

In order to estimate the final state effects it is essential to calculate the spectral function. We take the Eq. (10) as a starting point for studying how the final state spectral function effects the validity of IA. Since the excited electron in Compton scattering has a very high kinetic energy we will approximate the effects of the electron-electron interaction on the ejected electron using a simple free electron gas based model. This model can serve as a good estimate for these effects. It should be noticed that the only relevant quantity describing the free electron gas is its density n, which also determines the Fermi momentum (k_F) and the plasmon energy (ω_p). The electron gas density is more commonly characterized by the dimensionless parameter r_s associated to the electron-electron distance according to the formula $r_s=(3n/4\pi)^{1/3}$.

The spectral function $A(k,E)$ for an electron gas is given by

$$A(k,E)=\frac{1}{\pi}\left|\text{Im}\left[\frac{1}{E+\mu-k^2/2-\Sigma(k,E+\mu)}\right]\right|, \tag{11}$$

where μ is the chemical potential. We use Hedin's[14] GW approximation for the self-energy $\Sigma(k,E)$. As usual, the self-energy is separated into two parts

$$\Sigma^0(k,E)=\Sigma_{\text{HF}}(k)+\Sigma_s^0(k,E), \tag{12}$$

where $\Sigma_{\text{HF}}(k)$ is the energy-independent Hartree-Fock exchange potential and the energy dependence of the self-energy is included in $\Sigma_s^0(k,E)$. Following Ref. 23 we have used the notation $\Sigma^0(k,E)=\Sigma(k,E+E_0)$, where E_0 is the shift in the chemical potential $E_0=\mu-k_F^2/2$. When the self-energy is evaluated with the help of the Lindhard dielectric function (from now on referred to as G_0W_0), the final state electron's spectral function shows a double peak structure where one peak is due to the quasiparticle excitation (''main peak'') and the other is due to the quasiparticle-plasmon pair excitation (''satellite peak''). In order to approximate this effect we use a simple plasmon-pole model dielectric function

$$\text{Im}\left[\frac{1}{\varepsilon(k,E)}\right]=-\pi\omega_p\delta(E^2-\omega_p^2), \tag{13}$$

where $\omega_p=\sqrt{3/r_s^3}$ is the plasmon energy for the free electron gas. The advantage of choosing such a simple dielectric function is that an analytic result can be derived for the GWA self-energy (see appendix of Ref. 24). The final state electron's self-energy ($q>k_c+k_F$, where $k_c=k_f[\sqrt{1+2\omega_p/k_F^2}-1]$ is the plasmon cutoff momentum) in this approximation can be given in the terms of the Euler's dilogarithmic functions Li_2 (Refs. 25,26)

$$\Sigma_s^0(k,E)=\frac{\omega_p}{2\pi k}[\text{Li}_2(\alpha_-)-\text{Li}_2(-\alpha_-)+\text{Li}_2(-\alpha_+)-\text{Li}_2(\alpha_+)], \tag{14}$$

where $\alpha_\pm=q_c/(\sqrt{2(E-\omega_p+i\delta)}\pm k)$. In Ref. 24, q_c was set to be equal to k_c, but we will use it as a free parameter, which is adjusted to give the best approximation for the G_0W_0 spectral function for the final state electron. Li_2 satisfies a wide variety of identities that enable us to evaluate the function only for small arguments using a series expansion[25,26]

$$\text{Li}_2(z)=\sum_{n=1}^{\infty}\frac{z^n}{n^2},\quad |z|<1. \tag{15}$$

However, for the large momentum transfer case (and within the typical energy range of interest) usually $\alpha_->1$ and $\alpha_+<1$, and the following expression can be used:

$$\Sigma_s^0(k,E)=\frac{\omega_p}{\pi k}[-\chi_2(\alpha_-^{-1})-\chi_2(\alpha_+)+\pi^2/4-i\pi/2\ln\alpha_-], \tag{16}$$

where χ_2 are Legendre's chi functions. The singularity associated to the electron-plasmon coupling is included in the last term of Eq. (16). These two terms (assuming $q_c=k_c$) also give the large-k asymptotic behavior of the on-shell self-energy $\Sigma^0(k,k^2/2)$ mentioned in Ref. 8. For small arguments χ_2 has a series expansion[25,26]

$$\chi_2(z)=\sum_{n=0}^{\infty}\frac{z^{2n+1}}{(2n+1)^2}, \tag{17}$$

that converges rather quickly. To approximate the value for the chemical potential we need to evaluate E_0

$=\Sigma^0(k_f,k_f^2/2)$.[14] By introducing $y_\pm=\sqrt{2(E\pm\omega_p\mp i\delta)}$ the energy-dependent part of the self-energy can be written as[24]

$$\Sigma_s^0(k_f,E)=\frac{\omega_p}{2\pi k_f}\left[\mathrm{Li}_2\left(\frac{q_c}{y_- - k_f}\right)+\mathrm{Li}_2\left(\frac{-q_c}{y_- + k_f}\right)\right.$$
$$\left.-\mathrm{Li}_2\left(\frac{-q_c}{y_+ - k_f}\right)-\mathrm{Li}_2\left(\frac{q_c}{y_+ + k_f}\right)\right]. \qquad (18)$$

Using Eqs. (14), (16), and (18) the spectral function in Eq. (11) can be evaluated. We obtain the best agreement between the plasmon-pole (PP) model and G_0W_0 results when $q_c=2.6k_c$ for the electron densities considered here. The unphysically large value for q_c can be explained by the fact that the approximation for the dielectric function given in Eq. (13) does not have any contribution from the particle-hole pair continuum and its plasmon contribution does not have any dispersion. The Eqs. (14) and (16) are analytical approximations to the energy and momentum dependent self-energy for the large momentum values. They involve only elementary functions and functions that in practice can always be evaluated using series expansions [Eqs. (15) and (17)].

It is important to realize what is neglected when the dynamic structure factor is approximated with Eq. (10). As already mentioned, it does not take into account the contributions from the scattering from the plasmarons, which were neglected when the approximation (i) was made. Additionally, it does not include the electron-hole interaction (the so-called vertex-corrections), which were discussed in Ref. 22. Also the crystal potential can have a small effect on the final state electron, although the final state electron has kinetic energy of at least several hundreds of eV. All of these affect the observed valence electron Compton profile and should, in principle, be included before a quantitative comparison is made between the theory and the experiment. *First principles* studies on the effects of the electron-hole interaction in non-resonant inelastic x-ray scattering from valence electrons in moderate energy and momentum transfer regime have been conducted (see, for example Ref. 27, and references therein). However, in this work we are interested in the high momentum and energy transfer x-ray scattering, which is much harder to treat with the same accuracy. This is why we will concentrate on one specific effect, i.e. how does the final state electron-electron interaction smear the experimental Compton scattering spectra. In what follows, we will present the $\tilde{A}(k,E)$ in an energy scale where the zero energy is set to the center of gravity of the spectral function. In other words, we are not looking at the shift and the asymmetry introduced into the Compton profile by the spectral function convolution.

III. RESULTS AND DISCUSSION

We have extensively tested the PP-model introduced in the previous section for a range of electron densities. This includes the densities of most of the simple metals that have been studied using high resolution Compton scattering technique, specifically Be ($r_s=1.87$), Al ($r_s=2.07$), Li ($r_s=3.25$), and Na ($r_s=3.93$). The momentum transfer range was chosen from approximately 4 a.u. to 27 a.u. to cover the incident energies that have typically been used for the high resolution Compton scattering experiments (from 8 to 60 keV). These are summarized in Table I. As a first and an important step we have compared the results of the PP model to G_0W_0. Both methods seem to give almost identical spectral functions over the free electron densities and momentum transfer ranges mentioned above. This is emphasized at two different values of r_s in Fig. 1, which shows the comparison of the G_0W_0 and the PP model spectral functions for Li ($q=5.4$ a.u.) and Be ($q=14.9$ a.u.). Small differences can be observed, but the most important features, i.e., the overall width and the splitting and intensity ratio of the main and the satellite peaks are very close to each other. These small differences are further diminished in the actual Compton profiles after the convolution according to Eq. (10). Several tests confirm that the PP model is accurate within the abovemen-

TABLE I. Table showing the incident photon energy (ω_1), Compton peak energy (ω_2), scattering angle (θ), momentum transfer (q), and momentum resolution (Δp_z) for various recent high resolution Compton scattering experiments.

Experiment	Ref. 22	Ref. 21	Ref. 21	Ref. 21
ω_1	8.17 keV	10.28 keV	29.3 keV	56.2 keV
ω_2	7.92 keV	9.89 keV	26.3 keV	46.3 keV
θ	160°	165°	173°	162°
q	4.2 a.u.	5.4 a.u.	14.9 a.u.	27.1 a.u.
Δp_z	0.03 a.u.	0.02 a.u.	0.08 a.u.	0.16 a.u.

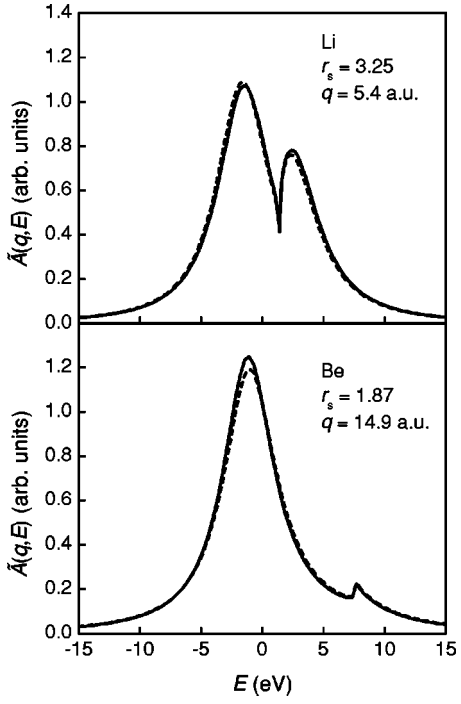

FIG. 1. Spectral functions calculated using the PP model discussed in the text (solid line) and G_0W_0 (dashed line). The values for r_s and q are indicated in the figure.

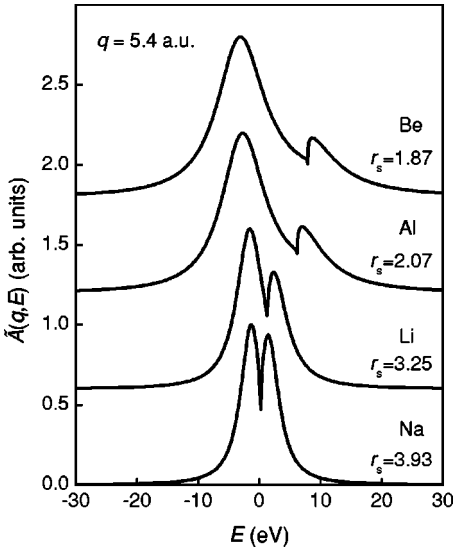

FIG. 2. Spectral functions calculated for various free electron densities corresponding to some simple metals. The momentum transfer value of 5.4 a.u. corresponds to a typical high resolution Compton scattering experiment carried out at around 10 keV (see Table I).

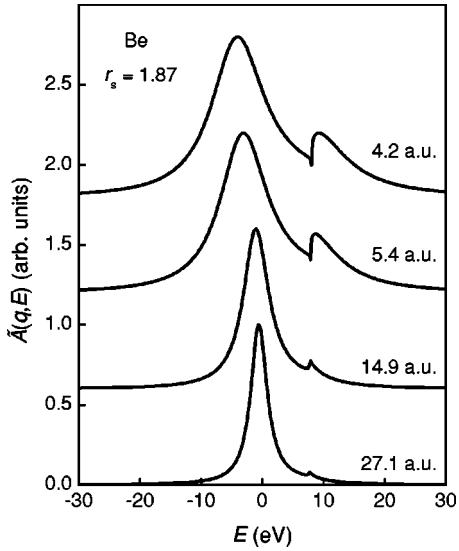

FIG. 3. Spectral functions calculated for free electron density of Be. The various momentum transfer values indicated in the figure correspond to typical Compton scattering experiments according to Table I.

tioned range of densities. As a function of momentum transfer the PP model works well up to $q<15$ a.u. but for the very high momentum transfers ($q>20$ a.u.) it slightly underestimates the width of the spectral function, i.e., the imaginary part of the self-energy. Due to the logarithmic singularity (see, for example, Ref. 24) in the imaginary part of the self-energy the spectral function evolves rather slowly to the well known Lorentzian shape. Only for extremely high momenta ($q>50$ a.u.) the spectral function can be approximated with a Lorentzian using the asymptotic limits for the quasiparticle peak width [see also[8] Eq. (9)]

$$\mathrm{Im}\ \Sigma(q,q^2/2)\rightarrow -\frac{\omega_p}{2q}\ln(q_c q/\omega_p) \tag{19}$$

and the quasiparticle shift [see also[8] Eq. (10)]

$$\mathrm{Re}\ \Sigma(q,q^2/2)\rightarrow -\pi\omega_p/(4q) \tag{20}$$

for both of which the next term behaves as q^{-2}. However, at this momentum transfer regime the role of the spectral function is negligible for the Compton scattering as we will show later. The approximation is slightly improved if the G_0W_0 value for the chemical potential is used. However, in this work we use the PP-model approximation for μ to make the work independent of the more laborious G_0W_0 approximation.

We have evaluated the spectral function for various electron densities and momentum transfers corresponding to some specific experimental setups used for the recent high resolution Compton scattering studies according to Table I. Since the shape of the spectral function depends only on r_s and q it is interesting at first to see the general trend as these parameters are varied. Figure 2 shows the spectral function calculated for different r_s corresponding to some free electron like low-Z metals. The momentum transfer of $q=5.4$ a.u. corresponds to an experimental setup at 10 keV (see Table I). It is rather surprising how much the spectral function changes its shape over such a relatively small range of electron densities. The same behavior is observed also at higher momentum transfer values. Based on this one would expect that the smearing of the Compton profile and the sharp Fermi breaks in the momentum density would be more pronounced for Be than for Na, for example.

The other important general tendency is the change of the spectral function as a function of the momentum transfer for a specific system. Figure 3 shows how the spectral function develops as the momentum transfer is increased for Be according to Table I. As the momentum transfer is increased the spectral function becomes narrower and the weight of the satellite peak reduces. This verifies the expectation that at higher momentum transfer values the final state effects become less important. This becomes even more striking when we convert the spectral function onto the momentum scale p_z, where the Compton profiles are generally presented, as shown in Fig. 4. Such a presentation is also very useful when one wants to estimate the final state effects compared with the momentum resolution obtainable at different incident photon energies given at Table I. It is obvious that at the low-energy experiments, where the best momentum resolution of about 0.02 a.u. is obtained, the smearing of the Compton profile due to the final state effects is overwhelming and clearly exceeds the experimental resolution. However, at the high incident photon energies the spectral function becomes narrower and the experimental resolution dominates. It should be noticed that the convolution of the theoretical Compton profile with the spectral function should be done (and is done here) on the energy scale according to Eq. (10). However, the spectral function does not change significantly over the Compton profile and we can quite reliably estimate the smearing effect of the spectral function by plotting it on the p_z scale as is done in Fig. 4.

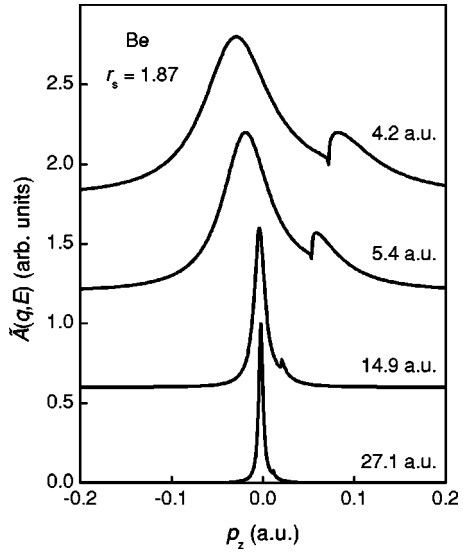

FIG. 4. Same spectral functions as in Fig. 3 but shown on the momentum scale p_z used for Compton profiles.

Recently there has been many experimental observations of anomalously large smearing of Compton profiles, especially when looking at the momentum density discontinuity at the Fermi break.[15,20,21] In many cases this has been attributed to an incomplete incorporation of the electron-electron correlation effects in the calculations of the momentum density.[29–31] Since with the model introduced in this paper it

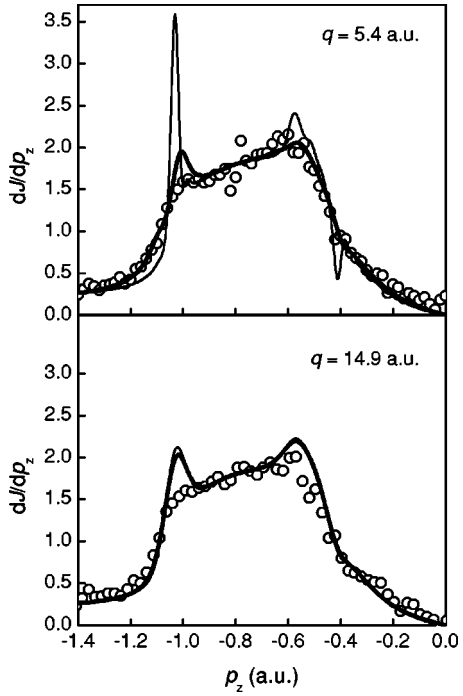

FIG. 5. First derivatives of the experimental (circles) and the theoretical Compton profiles (Ref. 21) with (thick solid line) and without (thin solid line) the spectral function correction for experiments carried out at two different momentum transfer values indicated in the figure. The momentum transfer values of 5.4 a.u. and 14.9 a.u. correspond to incident photon energies of about 10 and 30 keV according to Table I.

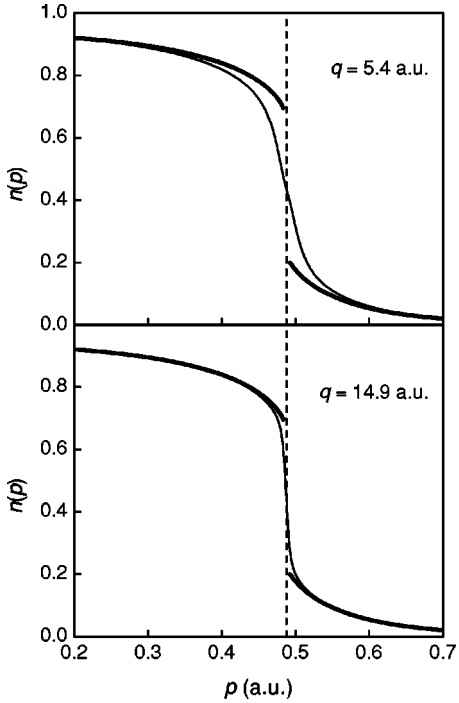

FIG. 6. The predicted smearing effect in the extracted momentum distribution function of Na due to the smearing of the experimental Compton profile caused by the final state effects. Two different momentum transfer values values of 5.4 a.u. and 14.9 a.u. correspond to incident photon energies of about 10 and 30 keV according to Table I. The momentum density is calculated according to Daniel and Vosko (Ref. 28).

is relatively easy to get a good estimate for the spectral function, it is rather interesting to look into the recent experimental results on Li, Be, and Na and see how much of the observed smearing could be explained by the spectral function.

Figure 5 shows the first derivative of the Be Compton profile measured at two different energy regimes corresponding to low and medium momentum transfers.[21] The LDA-based theoretical calculations including the Lam-Platzman correlation correction convoluted with the experimental resolution with and without final state effects are also shown in the same figure. At the low-energy (10 keV) experiment the final state effects are significant while in the experiment performed at 30 keV these effects are almost negligible. However, the experimental Fermi surface shows a remnant smearing, which cannot be explained by the final state effects discussed here. The remaining differences can be due to the inadequate description of the momentum density of the Lam-Platzman corrected LDA calculation. They can also be due to the exclusions of plasmaron contributions and the vertex-corrections discussed in the previous section. The same observation is supported by the recent study on Li, where most but not all of the observed smearing can be explained by the final state effects.[22] Additionally, similar conclusions have been made in connection to a detailed study of the Fourier transform of the Li Compton profile $B(\mathbf{r})$ measured at different incident photon energies.[32]

As a final example we look at sodium which is probably closest to free electron gas system of the examples discussed

here. Na has an almost perfectly spherical Fermi surface and therefore it is possible to extract the radial momentum density function directly from the experimental data and, more interestingly, the Fermi break. The Compton scattering technique can, in principle, serve as a unique tool to directly measure the jump of the momentum distribution function at the break, which will give the so-called quasiparticle renormalization constant Z_F. This parameter describes the strength of the electron-electron correlation and is of fundamental interest for many-body physics. There are several experimental studies where Z_F has been directly extracted from the Compton profiles[33] or by using fitting procedures assuming some functional behavior for the momentum density.[34] Figure 6 shows how the final state effects could be seen in the momentum distribution at two different experimental configurations. For the 10 keV experiment the smearing of the break is so severe that it would be very difficult to reconstruct the break directly or even by applying a fit for the momentum density. At 30 keV the smearing is significantly smaller and the extraction of Z_F could be feasible with a suitable model.

IV. CONCLUSION

We have studied the effects of the final state electron-electron interaction in Compton scattering in relation to the validity range of the widely used impulse approximation. For this purpose, we have introduced a relatively simple, but accurate enough, model for studying the role of the final state electron's spectral function. We have used a model spectral function, based on a free electron gas model, to study the effects on the Compton profile and its derivative as a function of momentum transfer. We found out that in this way we could explain a large part of the discrepancies found between the theory and the experimental results obtained with different momentum transfers. The remaining differences have to be attributed to the plasmaron effects, electron-hole interaction or to the inadequate description of the ground state momentum density.

The authors would like to acknowledge W. Schülke, C. Sternemann, and S. Huotari for discussions. This project was supported by the Academy of Finland (Grant No. 7379/40732/39182).

[1] L. Mendelsohn and F. Biggs, in *Proceedings of Inner-Shell Ionization, Atlanta, Georgia, 1972*, edited by R. W. Fink *et al.*, CONF-720404 (U.S. Atomic Energy Commission, Oak Ridge, TN, 1973), Vol. 3, p. 1142.
[2] B. J. Bloch and L. B. Mendelsohn, Phys. Rev. A **9**, 129 (1974).
[3] F. Gasser and C. Tavard, Phys. Rev. A **27**, 117 (1983).
[4] P. M. Bergstrom, T. Suric, K. Pisk, and R. H. Pratt, Phys. Rev. B **48**, 1134 (1993).
[5] A. Issolah, Y. Garreau, B. Levy, and G. Loupias, Phys. Rev. B **44**, 11 029 (1991).
[6] G. Bauer and J. R. Schneider, Phys. Rev. Lett. **52**, 2061 (1984).
[7] L. Lam and P. M. Platzman, Phys. Rev. B **9**, 5122 (1974).
[8] B. I. Lundqvist and C. Lyden, Phys. Rev. B **4**, 3360 (1971).
[9] W. C. Phillips and R. J. Weiss, Phys. Rev. **171**, 790 (1968).
[10] K. C. Pandey and L. Lam, Phys. Lett. **43A**, 319 (1973).
[11] P. Eisenberger, L. Lam, P. M. Platzman, and P. Schmidt, Phys. Rev. B **6**, 3671 (1972).
[12] Y. Takada and H. Yasuhara, Phys. Rev. B **44**, 7879 (1991).
[13] Y. Kubo, J. Phys. Soc. Jpn. **66**, 2236 (1997).
[14] L. Hedin, Phys. Rev. **139**, 796 (1965). The name the *GW* approximation arises from the fact that the electron self-energy involves the product of the electron Green's function *G* and the dynamically screened Coulomb interaction *W*.
[15] W. Schülke, G. Stutz, F. Wohlert, and A. Kaprolat, Phys. Rev. B **54**, 14 381 (1996).
[16] W. Schülke, J. Phys. Soc. Jpn. **68**, 2470 (1999).
[17] A. G. Eguiluz, W. Ku, and J. M. Sullivan, J. Phys. Chem. Solids **61**, 383 (2000).
[18] C. Filippi and D. M. Ceperley, Phys. Rev. B **59**, 7907 (1999).
[19] G. Stutz, F. Wohlert, A. Karpolat, W. Schülke, Y. Sakurai, Y. Tanaka, M. Ito, H. Kawata, N. Shiotani, S. Kaprzyk, and A. Bansil, Phys. Rev. B **60**, 7099 (1999).
[20] K. Hämäläinen, S. Manninen, C.-C. Kao, W. Caliebe, J. B. Hastings, A. Bansil, S. Kaprzyk, and P. M. Platzman, Phys. Rev. B **54**, 5453 (1996).
[21] S. Huotari, K. Hämäläinen, S. Manninen, S. Kaprzyk, A. Bansil, W. Caliebe, T. Buslaps, V. Honkimäki, and P. Suortti, Phys. Rev. B **62**, 7956 (2000).
[22] C. Sternemann, K. Hämäläinen, A. Kaprolat, A. Soininen, G. Döring, C.-C. Kao, S. Manninen, and W. Schülke, Phys. Rev. B **62**, R7687 (2000).
[23] B. I. Lundqvist, Phys. Kondens. Mater. **6**, 206 (1967).
[24] B. I. Lundqvist, Phys. Kondens. Mater. **6**, 193 (1967).
[25] L. Lewin, *Dilogarithms and Associated Functions* (North-Holland, Amsterdam, 1981).
[26] F. E. Harris, Phys. Rev. B **55**, 1820 (1997).
[27] W. A. Caliebe, J. A. Soininen, E. L. Shirley, C.-C. Kao, and K. Hämäläinen, Phys. Rev. Lett. **84**, 3907 (2000); J. A. Soininen and E. L. Shirley, Phys. Rev. B **61**, 16 423 (2000).
[28] E. Daniel and S. H. Vosko, Phys. Rev. **120**, 2041 (1960).
[29] Y. Sakurai, Y. Tanaka, A. Bansil, S. Kaprzyk, A. T. Stewart, Y. Nagashima, T. Hyodo, S. Nanao, H. Kawata, and N. Shiotani, Phys. Rev. Lett. **54**, 2252 (1995).
[30] M. Itou, Y. Sakurai, T. Ohata, A. Bansil, S. Kaprzyk, Y. Tanaka, H. Kawata, and N. Shiotani, J. Phys. Chem. Solids **59**, 99 (1998).
[31] T. Ohata, M. Itou, I. Matsumoto, Y. Sakurai, H. Kawata, N. Shiotani, S. Kaprzyk, P. E. Mijnarends, and A. Bansil, Phys. Rev. B **62**, 16 528 (2000).
[32] C. Sternemann (private communication).
[33] P. Eisenberger, L. Lam, P. M. Platzman, and P. Schmidt, Phys. Rev. B **6**, 3671 (1972).
[34] P. Suortti, T. Buslaps, V. Honkimäki, C. Metz, A. Shukla, Th. Tschentscher, J. Kwiatkowska, F. Maniawski, A. Bansil, S. Kaprzyk, A. S. Kheifets, D. R. Lun, T. Sattler, J. R. Schneider, and F. Bell, J. Phys. Chem. Solids **61**, 397 (2000).